Ionic and electronic correlations in liquid potassium from the electron-nucleus model

1993 J. Phys.: Condens. Matter 5 4315

(http://iopscience.iop.org/0953-8984/5/26/005)

J. Phys.: Condens. Matter 5 (1993) 4315–4324. Printed in the UK

Ionic and electronic correlations in liquid potassium from the electron–nucleus model

M Ishitobi† and J Chihara‡

† Department of Physics, Faculty of Science, Kanazawa University, Kanazawa, Ishikawa 920, Japan

‡ Department of Physics, Japan Atomic Energy Research Institute, Tokai, Ibaraki 319-11, Japan

Received 4 January 1993, in final form 12 March 1993

Abstract. By regarding a liquid metal as a mixture of electrons and nuclei, the quantal hypernetted-chain (QHNC) equations have been derived from the density-functional theory. These integral equations for the ion–ion and electron–ion radial distribution functions (RDFs) can give the electron distribution function of a neutral pseudoatom $\rho(r)$ and the effective interionic potential $v^{\mathrm{eff}}(r)$ self-consistently, using the atomic number Z_{A} as the only input data. We apply these equations to liquid potassium at 338 K. The ion–ion RDF $g_{\mathrm{II}}(r)$ and structure factor $S_{\mathrm{II}}(Q)$ obtained from QHNC agree with the experimental results from x-ray diffraction very well. The electron–ion RDF is calculated to be self-consistent with the effective interionic potential giving the ion–ion RDF in the QHNC framework. For comparison, the results of the pseudopotential method with Ashcroft's model potential (core radius $r_{\mathrm{C}} = 1.225$ Å) are also shown; this method can give the same ionic structures, but it provides slightly different electron distributions from the QHNC results. These differences between the QHNC and pseudopotential methods in the electron distribution are not observed in liquid sodium, and are attributed to the fact that the Ashcroft potential $w_{\mathrm{b}}^{\mathrm{AC}}(r)$ cannot appropriately approximate the direct correlation function $C_{\mathrm{el}}(r)$, which plays the role of a non-linear pseudopotential.

1. Introduction

As a traditional method of researching a simple liquid metal, a pseudopotential is used to set up an effective ion–ion interaction. In this model the electrons are accumulated around an ion according to a linear response to a pseudopotential. Therefore this treatment is valid only for a system with weak electron–ion interactions. As a result it is only used for simple liquid metals with weak electron–ion coupling. Dagens, Rasolt and Taylor (DRT) [1] calculated the non-linear electron distribution induced by an isolated ion in an electron gas in comparison with the linear response results. Thus, they concluded that the non-linear effect plays an important role even in alkali metals, and proposed a non-linear pseudopotential, which produces their non-linear electron distribution in the linear response form. Therefore it is very important to build up a pseudopotential in such a way as to produce a more realistic electron distribution, and it is meaningful to investigate the electron distribution in order to estimate the non-linear effect of the pseudopotential another way.

On the other hand, a set of integral equations for radial distribution functions (RDFs) have been proposed on the basis of the nucleus–electron mixture model using the density-functional theory (DFT) with the quantal hypernetted-chain (QHNC) approximation [2]. This formulation has already been applied to liquid metallic lithium [3] and sodium [4], and has been shown to yield the liquid structures of these metals in excellent agreement with

0953-8984/93/264315+10$07.50

experiment. In the light of the nucleus–electron mixture model, the more bound electrons in an ion, the more complicated the problem becomes in the calculation of the ion and electron distributions. One of the aims of this paper is to confirm that this QHNC formulation is applicable to liquid potassium with more bound electrons than sodium.

As was explained before, it is important for the construction of a pseudopotential to obtain knowledge of the distribution of screening electrons. But calculation of the electron–ion RDF in liquid metals is only possible by the QHNC method. Furthermore, it is difficult to establish the electron distribution around an ion experimentally, and only a few experiments have been performed to obtain electron distributions around an ion in liquid metals: no experiment has been carried out yet to research the valence electron distribution of liquid potassium. The QHNC method has an advantage in the fact that the electron–ion RDF, ion–ion RDF, non-linear pseudopotential and effective interionic potential are determined at the same time self-consistently from the atomic number Z_A as the only input.

The layout of this paper is as follows. We give an outline of the QHNC method for a liquid metal in section 2. In section 3 the implementation of the QHNC method to liquid potassium is overviewed, and we report the results of the calculation in section 4. In the last section we discuss our results and draw our conclusions.

2. Summary of formulation

In this section we recapitulate the QHNC formulation. Details are to be found in [2], [3] and [5]. In the first place a liquid metal is treated as an electron–ion mixture. Here we assume that ions in a liquid metal are classical particles with a charge Z_I and average density n_0^I, while the electrons form a quantum fluid with average density n_0^e. Because the ions behave as classical particles, the ion–ion and electron–ion RDFs are shown to be identical with the ionic and electronic density distributions, respectively, around a fixed ion in a liquid metal. With the help of the DFT, each RDF can be exactly represented by the density distribution function $n_i^0(r|v_{il}^{\mathrm{eff}})$ of a non-interacting system under an effective external potential $v_{il}^{\mathrm{eff}}(r)(i = \mathrm{e}, \mathrm{I})$:

$$g_{\mathrm{II}}(r) = n_{\mathrm{I}}^0(r|v_{\mathrm{II}}^{\mathrm{eff}})/n_0^{\mathrm{I}} = \exp[-\beta v_{\mathrm{II}}^{\mathrm{eff}}(r)] \tag{1}$$

$$g_{\mathrm{eI}}(r) = n_{\mathrm{e}}^0(r|v_{\mathrm{eI}}^{\mathrm{eff}})/n_0^{\mathrm{e}}. \tag{2}$$

In the above the effective potential $v_{il}^{\mathrm{eff}}(r)$ is written explicitly in terms of the bare potential $v_{il}(r)$, the direct correlation functions (DCFs) $C_{ij}(r)$ and the bridge function $B_{il}(r)$:

$$v_{il}^{\mathrm{eff}}(r) = v_{il}(r) - \Gamma_{il}(r)/\beta - B_{il}(r)/\beta \tag{3}$$

$$\Gamma_{il}(r) \equiv \sum_{\ell} \int C_{i\ell}(|\boldsymbol{r} - \boldsymbol{r}'|) n_0^{\ell}[g_{\ell l}(r') - 1]\,\mathrm{d}\boldsymbol{r}'. \tag{4}$$

Moreover, we have the Ornstein–Zernike (OZ) relations for the electron–ion system [5]:

$$g_{\mathrm{II}}(r) - 1 = C_{\mathrm{II}}(r) + \Gamma_{\mathrm{II}}(r) \tag{5}$$

$$g_{\mathrm{eI}}(r) - 1 = \hat{B}C_{\mathrm{eI}}(r) + \hat{B}\Gamma_{\mathrm{eI}}(r). \tag{6}$$

Here $\hat{B}$ is an operator defined for an arbitrary real number α with the Fourier-transformation operator $\mathcal{F}_Q$ as follows:

$$\mathcal{F}_Q[\hat{B}^{\alpha} f(r)] = (\chi_Q^0)^{\alpha} \mathcal{F}_Q[f(r)] \tag{7}$$

where χ_Q^0 is the density–density response function of a non-interacting electron gas. Equations (1), (2), (5) and (6) form a set of integral equations for correlations in an electron–ion mixture if some approximations are introduced, as will be mentioned later.

From the definition of the structure factor $S_{\mathrm{il}}(Q)$ [5], we can obtain an exact relation in real space by the use of the inverse Fourier transformation

$$n_0^{\mathrm{e}} g_{\mathrm{el}}(r) = \rho(r) + n_0^{\mathrm{I}} \int \rho(|r - r'|) g_{\mathrm{II}}(r')\, \mathrm{d}r' \tag{8}$$

with

$$\rho(Q) \equiv n_0^{\mathrm{e}} C_{\mathrm{el}}(Q) \chi_Q^0 / [1 - n_0^{\mathrm{e}} C_{\mathrm{ee}}(Q) \chi_Q^0]. \tag{9}$$

Equation (9) states that the RDF $g_{\mathrm{el}}(r)$ can be expressed exactly as a superposition of neutral pseudoatoms with the electron distribution $\rho(r)$ around an ion. On the other hand, in the pseudopotential method, the charge distribution $\rho(Q)$ of a pseudoatom is represented by the following linear response formula:

$$\begin{aligned} \rho(Q) &= -n_0^{\mathrm{e}} \beta w_{\mathrm{b}}(Q) \chi_Q^{\mathrm{jell}} \\ &= -n_0^{\mathrm{e}} \beta w_{\mathrm{b}}(Q) \chi_Q^0 / [1 + n_0^{\mathrm{e}} \beta v_{\mathrm{ee}}(Q)(1 - G^{\mathrm{jell}}(Q)) \chi_Q^0] \end{aligned} \tag{10}$$

using a pseudopotential $w_{\mathrm{b}}(Q)$, the density response function χ_Q^{jell} and the local-field correction (LFC) $G^{\mathrm{jell}}(Q)$ in the electron jellium model. While equation (10) is valid only for systems with weak electron–ion correlation, equation (9) is an exact relation for the electron–ion system. Comparing these equations, it is apparent that the following two replacements make two equations (9) and (10) identical with each other:

$$C_{\mathrm{ee}}(Q) \simeq -\beta v_{\mathrm{ee}}(Q)(1 - G^{\mathrm{jell}}(Q)) \tag{11}$$

$$C_{\mathrm{el}}(Q) \simeq -\beta w_{\mathrm{b}}(Q). \tag{12}$$

Thus, we can understand from (11) that the electron–electron DCF $C_{\mathrm{ee}}(Q)$ is approximated in terms of the LFC $G^{\mathrm{jell}}(Q)$ of the jellium model instead of the LFC in the ion–electron mixture. From (12), it is seen that the electron–ion DCF $C_{\mathrm{el}}(Q)$ plays the role of a non-linear pseudopotential.

In determining a liquid structure, a liquid metal can be regarded as a quasi-one-component system which consists of ions alone. In this model the existence of electrons is taken into account only in the construction of an effective interionic potential $v^{\mathrm{eff}}(r)$, which can be rewritten as

$$v_{\mathrm{II}}^{\mathrm{eff}}(r) = v^{\mathrm{eff}}(r) - \gamma(r)/\beta + B_{\mathrm{II}}(r)/\beta \tag{13}$$

with the definition

$$\beta v^{\mathrm{eff}}(Q) \equiv \beta v_{\mathrm{II}}(Q) - C_{\mathrm{el}}^2(Q) n_0^{\mathrm{e}} \chi_Q^0 / [1 - n_0^{\mathrm{e}} C_{\mathrm{ee}}(Q) \chi_Q^0] \tag{14}$$

in terms of the DCF $C(r)$ of the one-component system:

$$n_0^{\mathrm{I}} C(Q) \equiv 1 - 1/S_{\mathrm{II}}(Q) \tag{15}$$

and

$$\gamma(r) \equiv n_0^{\mathrm{I}} \int C(|r-r'|)[g_{\mathrm{II}}(r')-1]\,\mathrm{d}r'. \tag{16}$$

Up to now, we have not considered the inner structure of an ion. In fact an ion consists of a nucleus and some bound electrons. Now, the bare potential $\tilde{v}_{\mathrm{eI}}(r)$ is derived as

$$\tilde{v}_{\mathrm{eI}}(r) = v_{\mathrm{eN}}(r) + \int v_{\mathrm{ee}}(|r-r'|)n_{\mathrm{e}}^{\mathrm{b}}(r')\,\mathrm{d}r' + \mu_{\mathrm{XC}}(n_{\mathrm{e}}^{\mathrm{b}}(r)+n_0^{\mathrm{e}}) - \mu_{\mathrm{XC}}(n_0^{\mathrm{e}}) \tag{17}$$

by regarding a liquid metal as a mixture of nuclei and electrons [3]. Here $n_{\mathrm{e}}^{\mathrm{b}}(r)$ denotes the bound electron distribution, and $\mu_{\mathrm{XC}}(n)$ is the exchange–correlation potential. In this approach we assume that there is no overlapping of bound electrons among ions: accordingly we can determine simply the ionic valency Z_{I} from $n_{\mathrm{e}}^{\mathrm{b}}(r)$ as

$$Z_{\mathrm{I}} = Z_{\mathrm{A}} - \int n_{\mathrm{e}}^{\mathrm{b}}(r)\,\mathrm{d}r. \tag{18}$$

3. Application to liquid potassium

The set of equations (1), (2), (5) and (6) for the RDFs $g_{il}(r)$ and the DCF $C_{ij}(r)$ do not yet form a closed set to determine themselves. In order to obtain closed equations, we introduce the following approximations.

(a) The electron–electron DCF $C_{\mathrm{ee}}(Q)$ is approximated in terms of the jellium LFC $G^{\mathrm{jell}}(Q)$ proposed by Geldart and Vosko [6]:

$$G^{\mathrm{jell}}(Q) = q^2/(2q^2+4g) \tag{19}$$

with $q = Q/Q_{\mathrm{F}}$, $g = 1/(1+0.0155\alpha\pi r_{\mathrm{S}})$, $\alpha = (4/9\pi)^{1/3}$, $r_{\mathrm{S}} = (3/4\pi n_0^{\mathrm{I}})^{1/3}$ and Q_{F} the Fermi wave-number.

(b) The ion–ion bridge function $B_{\mathrm{II}}(r)$ in (3) is approximated by $B_{\mathrm{PY}}(r;\eta)$ of the Percus–Yevick equation for hard spheres with diameter σ:

$$B_{\mathrm{II}}(r) \simeq B_{\mathrm{PY}}(r;\eta) \tag{20}$$

with a packing fraction parameter defined by $\eta \equiv \pi n_0^{\mathrm{I}}\sigma^3/6$.

(c) The electron–ion bridge function $B_{\mathrm{eI}}(r)$ is neglected:

$$B_{\mathrm{eI}}(r) = 0. \tag{21}$$

(d) The ion–ion bare potential $v_{\mathrm{II}}(r)$ is taken as coulombic:

$$v_{\mathrm{II}}(r) = Z_{\mathrm{I}}e^2/r \tag{22}$$

because the overlapping of ions is assumed to be zero.

The approximation (b) indicates that the spirit of the modified HNC (MHNC) [7] is applied to the ion–ion correlation, and (c) denotes that the HNC approximation is used in the electron–ion correlation. The exchange–correlation potential $\mu_{XC}(n)$ in (17) is taken to be that proposed by Gunnarsson and Lundqvist [8]:

$$\mu_{XC}(r_S) = -(2/\pi\alpha r_S)[1 + 0.0545 r_S \ln(1 + 11.4/r_S)] \qquad \text{(Ryd)}. \tag{23}$$

Under these approximations equations (1), (2), (5) and (6) generate a coupled set of integral equations for the DCF $C_{eI}(r)$ and the ion–ion RDF $g_{II}(r)$ in the following forms: the equation for the non-linear pseudopotential $C_{eI}(r)$

$$\widehat{B}C_{eI}(r) = n_e^0(r|\,\tilde{v}_{eI} - \Gamma_{eI}/\beta)/n_0^e - 1 - \widehat{B}\Gamma_{eI}(r) \tag{24}$$

which determines the effective interaction $v^{eff}(r)$ for the one-component fluid through (14) if the RDF $g_{II}(r)$ is provided, and the equation for the DCF $C(r)$ in the one-component fluid

$$C(r) = \exp[-\beta v^{eff}(r) + \gamma(r) + B_{II}(r)] - 1 - \gamma(r) \tag{25}$$

which can give the ion–ion RDF $g_{II}(r)$ for the one-component fluid interacting via $v^{eff}(r)$ evaluated by (14).

The atomic number Z_A and the ionic valency Z_I of liquid potassium are 19 and 1 respectively, so that $n_0 \equiv n_0^e = n_0^I$. A potassium ion in the ground state consists of a nucleus and 18 bound electrons in the five states 1s, 2s, 2p, 3s and 3p. The state of liquid potassium can be specified by two parameters: the plasma parameter $\Gamma \equiv \beta e^2/a$ and $r_S \equiv a/a_B$ with the average spherical radius $a = (3/4\pi n_0)^{1/3}$.

In order to solve the integral equations in a self-consistent way, it is important to choose the initial data. Since the values of the parameters are large ($\Gamma \simeq 180, r_S \simeq 5$) for liquid potassium near the melting point (336.8 K), we cannot obtain a convergent solution for this system if the initial data are not enough close to the real solution. The method of making the initial data and the set-up of the grid in the integration of the wave equation are the same as were used for liquid sodium [4]. The packing fraction η in the bridge function $B_{PY}(r;\eta)$ was determined by the Lado criterion [9] in the case of liquid sodium. In the present calculation it is chosen to fit the calculations to the experiments. We discuss η later.

4. Results of calculation

In this section we show the ion and electron distributions of liquid metallic potassium at 338 K near the melting point calculated by the QHNC method. At this temperature liquid potassium has the number density $n_0 = 1.27 \times 10^{-2}$ Å^{-3} [10]: this yields the plasma parameter $\Gamma = 185.9$ with $r_S = 5.024$. Here we set the packing fraction in (20) $\eta = 0.445$ to give the best fit of the ion–ion structure factor $S_{II}(Q)$ and the RDF $g_{II}(r)$ to experiment. As already mentioned, the electron–ion DCF $C_{eI}(r)$ in (14) plays the role of a non-linear pseudopotential. So if we replace the DCF $C_{eI}(r)$ by a model potential, we can obtain the ion–ion RDF $g_{II}(r)$ through (25), and the electron distribution of a pseudoatom $\rho(r)$ from (9) in this approximation. For comparison between the QHNC and pseudopotential methods, we calculate the ion–ion and electron–ion RDFs, $\rho(r)$ and the effective ion–ion interaction under the same state parameters with use of Ashcroft's model potential $w_b^{AC}(r)$:

$$C_{eI}(r) = -\beta w_b^{AC}(r) = \begin{cases} 0 & (r \leqslant r_C) \\ \beta Z_I e^2/r & (r > r_C) \end{cases} \tag{26}$$

with core radius $r_C = 1.225$ Å.

Firstly the ion–ion structure factors $S_{II}(Q)$ are shown in figure 1 for comparison with the experiments by Greenfield and co-workers [11] (open circles) and by Huijben and van der Lugt [12] (filled circles). The full curve denotes the result obtained by the QHNC method with $\eta = 0.445$. Our self-consistent $S_{II}(Q)$ agrees with the x-ray diffraction experiments of Greenfield *et al* and Huijben and van der Lugt excellently. The QHNC structure factor (full curve) has a higher first peak than that of Greenfield *et al*, but agrees with that of Huijben and van der Lugt. Near the second peak the QHNC result deviates from both experiments a little. There is a similar deviation in liquid sodium and in another calculation for liquid potassium [13]. Moreover the result of the pseudopotential method, based on Ashcroft's model potential (triangles), shows good agreement with the QHNC result using the packing fraction $\eta = 0.46$. As the values of $S_{II}(Q = 0)$ we obtain 0.0206 from the QHNC method and 0.0282 from the pseudopotential method. X-ray diffraction experiments give 0.0247 (Greenfield *et al*) and 0.0241 (Huijben and van der Lugt) for $S_{II}(0)$.

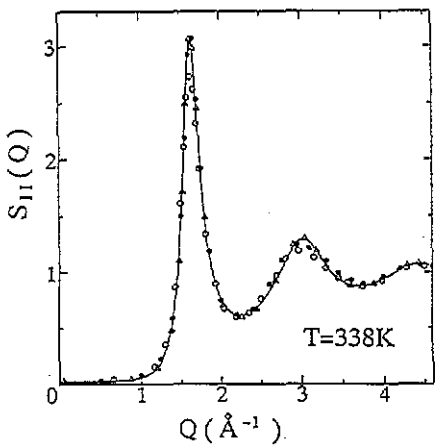

Figure 1. The ion–ion structure factor $S_{II}(Q)$ calculated for liquid potassium at 338 K with the state parameters $\Gamma = 185.9$ and $r_S = 5.024$. Full curve, the full self-consistent QHNC calculation; open circles, x-ray diffraction data of Greenfield *et al* [11]; filled circles, x-ray diffraction data of Huijben and van der Lugt [12]; triangles, pseudopotential calculation using Ashcroft's potential with the core radius $r_C = 1.225$ Å.

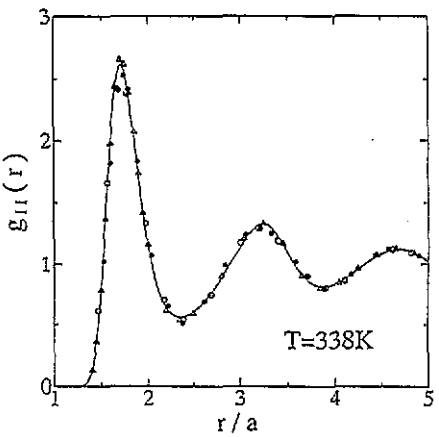

Figure 2. The ion–ion RDFs $g_{II}(r)$ of liquid potassium at 338 K, calculated by the QHNC method (full curve) and by the Monte Carlo method [14] (open circles). The filled circles denote the RDF $g_{II}(r)$ obtained by Fourier transformation from the structure factor $S_{II}(Q)$ obtained by Huijben and van der Lugt. The triangles show the RDF $g_{II}(r)$ calculated using Ashcroft's potential.

Secondly the ion–ion RDF $g_{II}(r)$, the inverse Fourier transformation of the structure factor $S_{II}(Q)$ of figure 1, is shown in figure 2. Our result (full curve) agrees with the RDF of Huijben and van der Lugt [12] (filled circles) obtained by the inverse Fourier transformation of $S_{II}(Q)$ with a slightly lower first peak. The Monte Carlo (MC) RDF (open circles) of Murphy [14] agrees with the QHNC result very well: the structure factor $S_{II}(Q)$ obtained from Murphy's RDF shows good agreement with the experimental one of Greenfield *et al*. The RDF from the pseudopotential method (triangles) fits to the QHNC result with a slightly higher first peak.

Figure 3 shows the effective interionic potentials $v^{eff}(r)$ determining the ion–ion RDFs $g_{II}(r)$. The QHNC result is denoted by the full curve. The potentials used in the MC calculation of Murphy (open circles) and the MD simulation of Jank and Hafner [15] (filled

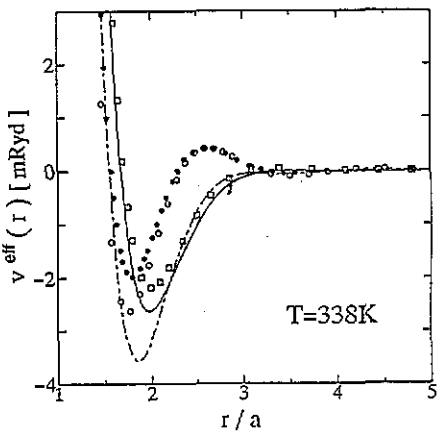

Figure 3. The effective interionic potential $v^{\text{eff}}(r)$ of liquid potassium at 338 K calculated by the QHNC method (full curve), by the pseudopotential method (chain curve) and using the jellium vacancy model (squares). The filled circles represent the potential used in the MD simulation of Jank and Hafner [15] and the open circles show that used in the MC calculation of Murphy [14].

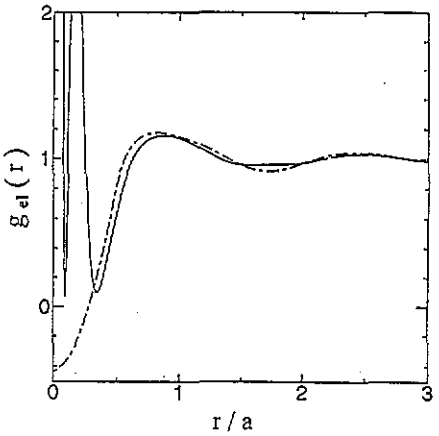

Figure 4. The electron–ion RDF $g_{\text{el}}(r)$ for liquid potassium, calculated by the QHNC method (full curve) and by the pseudopotential method using Ashcroft's potential (chain curve).

circles) have lower limits at the same position. These potentials show similar behaviour at the repulsive region and shifted lower limits in depth. In spite of shifted lower limits, these potentials give similar $g_{\text{II}}(r)$ and $S_{\text{II}}(Q)$. As seen in figure 2, Murphy's potential gives an RDF $g_{\text{II}}(r)$ in good agreement with the experimental $g_{\text{II}}(r)$. The potential of Jank and Hafner gives the structure factor $S_{\text{II}}(Q)$ in good agreement with that of Huijben and van der Lugt. Their potential is obtained from a pseudopotential constructed on the basis of the criterion proposed by Cohen and Heine [16]. The potential obtained by the pseudopotential method (chain curve) and using the jellium vacancy model for ions (squares) are exhibited in comparison with the QHNC potential. The jellium vacancy model comes from the QHNC formulation by the use of an approximation that the ion–ion RDF $g_{\text{II}}(r)$ is replaced by a step function in the expression for $v_{\text{el}}^{\text{eff}}(r)$ (4). The jellium vacancy model is essentially equivalent to DRT's treatment in the evaluation of a pseudopotential. DRT's potential, however, has a minimum at a position nearer the origin than that in the jellium vacancy model. This potential is very sensitive to the choice of the LFC $G^{\text{jell}}(Q)$. On the other hand, the RDF $g_{\text{II}}(r)$ does not depend on the LFC $G^{\text{jell}}(Q)$ significantly. A different LFC $G^{\text{jell}}(Q)$ changes the position of the minimum, but does not reflect on the behaviour of the repulsive region, which plays an important role in determination of the RDF $g_{\text{II}}(r)$. The influence of the LFC $G(Q)$ on the effective potential $v^{\text{eff}}(r)$ is discussed in the next section.

Up to this point we have shown the quantities related to the ion–ion correlation; from here we show the quantities related to the electron–ion correlation. First, the electron–ion RDF $g_{\text{el}}(r)$ is displayed in figure 4. The full curve represents the RDF $g_{\text{el}}(r)$ obtained by the QHNC method, while the chain curve denotes that obtained by the pseudopotential method using Ashcroft's model potential. In the core region these RDFs behave differently. In particular, the RDF of the QHNC oscillates rapidly near the origin. In order to observe this situation, the RDF $g_{\text{el}}(r)$ is magnified for the region $r/a < 0.5$ in figure 5. There are three dips (at $r/a = 0.025$, 0.0875 and 0.35) in this region. The triangles in figure 5 indicate

the positions of the average radii of the ith bound electron state in an ion (i = 1s, 2s, 2p, 3s and 3p). The average radius in the the ith state is defined by $\sqrt{\langle r_i^2 \rangle} = \sqrt{\int r^2 \psi_i(r)^2 \, dr}$. From this figure we find out an interesting fact that each dip in the electron–ion RDF lies near the positions of the average radii of bound electrons in an ion. The nearest dip to the origin represents the repulsion caused by two electrons in the 1s state. The middle dip reflects that of eight electrons in the 2s and 2p states, and the outer dip denotes that of eight electrons in the 3s and 3p states. It is suggested that the number of related electrons determines the depth of a dip and that the width of a dip depends on the expanse of the relative orbital. Therefore the 1s electrons make a tight and shallow dip, while the 3s and 3p electrons make broad and deep dips. In figure 4 the RDF $g_{el}(r)$ by Ashcroft's model potential (chain curve) has a large deviation in the core region, and furthermore has a slight but meaningful deviation outside the core region in comparison with the QHNC result. It is interesting to note that this difference outside the core region is not found in liquid sodium. The electron–ion RDF $g_{el}(r)$ converges upon unity more quickly at large r than the ion–ion RDF $g_{II}(r)$. This fact means that the electron–ion correlation decays rapidly, and suggests the validity of neglecting the electron–ion bridge function (equation (23)).

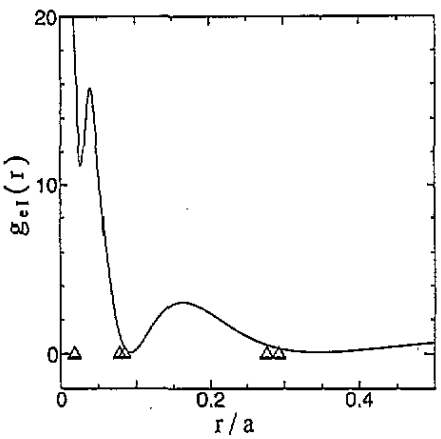

Figure 5. The electron–ion RDF $g_{el}(r)$ magnified in the core region, obtained from the QHNC method (full curve). The triangles are plotted to point out the average radii of bound electrons.

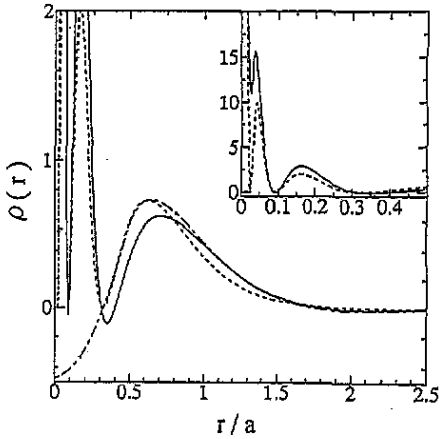

Figure 6. The screening electron distribution $\rho(r)$ of a neutral pseudoatom calculated by the QHNC method (full curve) and by the pseudopotential method (chain curve). The broken curve shows the density of 4s electrons of a free atom. Furthermore for the purpose of demonstrating the inside behaviour, $\rho(r)$ is magnified in the inset.

Figure 6 exhibits the screening electron distribution of a neutral pseudoatom $\rho(r)$ scaled by n_0. The QHNC distribution $\rho(r)$ (full curve) has three dips (to show the inner dip, $\rho(r)$ near the origin is magnified in the inset), and shows similar behaviour to that of a free atom (broken curve) with three nodes. The positions of the dips (r/a = 0.025, 0.0875 and 0.35) in the QHNC $\rho(r)$ are coincident with that of the RDF $g_{el}(r)$. Similarly to $g_{el}(r)$, these dips reflect the inner structure of an ion. The distribution $\rho(r)$ from the pseudopotential method (chain curve) agrees with that from the QHNC method at large r ($r/a > 1$), but disagrees at small r ($r/a < 1$). By contrast it is to be noted that in liquid sodium the values of $\rho(r)$ agree in the wider range $r/a > 0.5$.

5. Conclusion and discussion

We have shown ionic and electronic correlations in liquid potassium at 338 K calculated by the QHNC method based on the electron–nucleus model. The bound electron distribution of an ion is determined to be consistent with the valence electron and ionic distributions around it: the effective potential $v_{eI}^{eff}(r)$ can support only five bound states (1s, 2s, 2p, 3s and 3p) with the ionic valency being $Z_I = 1$ due to a 4s valence state electron. As shown in figures 1 and 2, the RDF $g_{II}(r)$ and structure factor $S_{II}(Q)$ obtained by the QHNC method agree with the experimental ones excellently. On the other hand the RDF $g_{eI}(r)$ and the distribution $\rho(r)$ can be taken as reliable, since these are determined to be consistent with the ion–ion RDF $g_{II}(r)$, which agrees with experiment.

In this calculation, we introduced two quantities from outside the QHNC self-consistent formulation: the exchange–correlation potential $\mu_{XC}(n)$ in (17) and the LFC $G^{jell}(Q)$ in (19). The effective interionic potential $v^{eff}(r)$ is influenced by the LFC $G(Q)$ sensitively. The LFC $G^{jell}(Q)$ must satisfy some conditions for electrons in the jellium model. Unfortunately these conditions for the jellium model do not ensure that the LFC is valid for electrons in a real liquid metal taken as an ion–electron mixture. So we have no criteria for the selection of LFC $G(Q)$ in a liquid metal taking account of the presence of ions. In order to examine the influence of the LFC on the effective potential, we calculated the effective potentials using four different LFCs: of Geldart and Vosko, of Vashishta and Singwi [17], of Taylor [18] and of Utsumi and Ichimaru [19]. These four potentials show large disagreements with each other. The influence of the LFC on the effective potential has a similar tendency as is shown by Hafner [20]. In spite of the large deviations among the effective potentials due to the LFC, the structure factor $S_{II}(Q)$ and the RDF $g_{II}(r)$ are not significantly dependent on the choice of LFC $G^{jell}(Q)$. At the present stage we cannot say which LFC $G^{jell}(Q)$ is best for liquid potassium.

We have tried to determine the packing fraction η by using the variational MHNC (VMHNC) [21], which gives $\eta = 0.47$; at this value the structure factor $S_{II}(Q)$ and the RDF $g_{II}(r)$ have a fairly high first peak in the QHNC calculation. Therefore the parameter η is determined so as to fit the structure factor $S_{II}(Q)$ to the experiment of Huijben and van der Lugt overall. On the other hand, the VMHNC method gives η=0.46 for Ashcroft's potential.

As shown in figures 4 and 6, the electron distribution obtained by the QHNC method is quite different from that by obtained by Ashcroft's model potential in liquid potassium. Such deviations have not appeared in liquid sodium [4]. We cannot find the core radius r_C of the pseudopotential to yield the best fit to the QHNC $\rho(Q)$ for a liquid potassium. The essential difference between the pseudopotential and QHNC methods lies in the determination of the pseudopotential $w_b(r)$: in the QHNC method $w_b(r)$ is determined to be consistent with the density distribution of a pseudoatom $\rho(r)$, while in the pseudopotential method a pseudopotential $w_b(r)$ is approximated by Ashcroft's model potential with a proper choice of the core radius r_C as input data. The comparison of both pseudopotentials in liquid potassium and sodium is exhibited in figure 7. In liquid sodium the non-linear pseudopotential $-C_{eI}(r)/\beta$ (lower full curve) from the QHNC method behaves similarly to Ashcroft's model potential (lower chain curve) near the minimum. On the other hand, in liquid potassium the non-linear pseudopotential $-C_{eI}(r)/\beta$ (upper full curve) has a shallower minimum than Ashcroft's potential (upper chain curve). It is suggested that this difference causes the deviations from the QHNC result in the electronic distribution $g_{eI}(r)$ (figure 4) and $\rho(r)$ (figure 6) for the case of potassium. Ashcroft's model potential $w_b^{AC}(r)$ has a constant value for the inside core radius r_C (almost inside an ion), so it disregards the fine structure

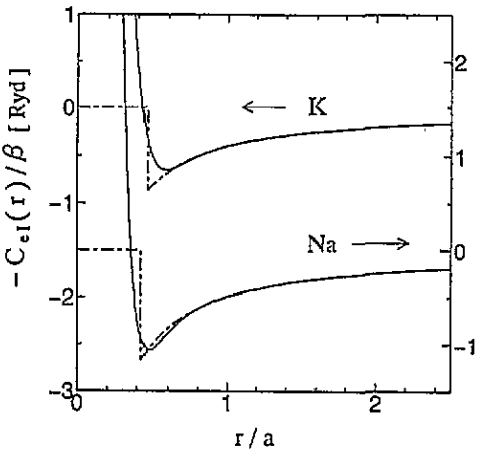

Figure 7. The electron–ion DCF $C_{el}(r)$, a non-linear pseudopotential, of liquid potassium (upper full curve) and of liquid sodium (lower full curve) calculated by the QHNC method. Though the DCF $C_{el}(r)$ oscillates rapidly in the core region, the vibrations are masked in order to make a simple figure. Ashcroft's model potentials $w_b^{AC}(r)$ are plotted as the chain curves for liquid potassium with a core radius $r_C = 1.225$ Å, and for liquid sodium with core radius $r_C = 0.905$ Å. The upper curves of potassium are measured against the left vertical axis, while the lower curves of sodium are measured against the right axis.

due to bound electrons. For the reason that an ion has more bound electrons (3s, 3p) in liquid potassium than in liquid sodium, the rough approximation to the core-electron effect in Ashcroft's potential may cause the deviations of the electron distribution in the case of potassium. In order to check this guess it is necessary to carry out the same calculation for some heavier elements.

References

[1] Rasolt M and Taylor R 1975 *Phys. Rev.* B **11** 2717
Dagens L, Rasolt M and Taylor R 1975 *Phys. Rev.* B **11** 2726
[2] Chihara J 1986 *Phys. Rev.* A **33** 2575
[3] Chihara J 1989 *Phys. Rev.* A **40** 4507
[4] Ishitobi M and Chihara J 1992 *J. Phys.: Condens. Matter* **4** 3679
[5] Chihara J 1984 *J. Phys. C: Solid State Phys.* **17** 1633
[6] Geldart D J W and Vosko J H 1966 *Can. J. Phys.* **44** 2137
[7] Rosenfeld Y and Ashcroft N W 1979 *Phys. Rev.* A **20** 1208
[8] Gunnarsson O and Lundqvist B I 1976 *Phys. Rev.* B **13** 4243
[9] Lado F, Foiles S M and Ashcroft N W 1983 *Phys. Rev.* A **28** 2374
[10] Hausleitner C and Hafner J 1988 *J. Phys. F: Met. Phys.* **18** 1013
[11] Greenfield A J, Wellendorf J and Wiser N 1971 *Phys. Rev.* A **4** 1607
[12] Huijben M J and van der Lugt W 1979 *Acta Crystallogr.* A **35** 431
[13] Lai S K, Li W and Tosi M P 1990 *Phys. Rev.* A **42** 7289
[14] Murphy R D 1977 *Phys. Rev.* A **15** 1188
[15] Jank W and Hafner J 1991 *J. Phys.: Condens. Matter* **3** 6947
[16] Cohen M H and Heine V 1961 *Phys. Rev.* **122** 1821
[17] Vashishta P and Singwi K S 1972 *Phys. Rev.* B **6** 875
[18] Taylor R 1978 *J. Phys. F: Met. Phys.* **8** 1699
[19] Utsumi K and Ichimaru S 1982 *Phys. Rev.* A **26** 603
[20] Hafner J 1987 *From Hamiltonians to Phase Diagrams* (Berlin: Springer)
[21] Rosenfeld Y 1986 *J. Stat. Phys.* **42** 437
Gonzalez L E, Gonzalez D J and Silbert M 1991 *Physica* B **168** 39